

Holographic nondiverging hollow beam

Hee S. Lee, B. W. Stewart, K. Choi, and H. Fenichel

Department of Physics, University of Cincinnati, Cincinnati, Ohio 45221-0011

(Received 4 August 1993)

A simple holographic technique is used to generate a nondiverging hollow beam, which is similar to a J_1 Bessel beam. The hollow beam is obtained from a Gaussian beam with a high conversion efficiency (greater than 50%). We describe briefly the merit of this hollow beam, which has potential applications in particle collimation.

PACS number(s): 42.60.-v, 42.25.Bs, 42.25.Md, 42.40.My

INTRODUCTION

Methods for generation of a J_0 beam, the first order of the first kind of Bessel beam, are well established [1-8]. A J_1 beam, the second-order Bessel beam, and higher-order beams can also be obtained using computer-generated holograms [8]. However, these computer-generated beams have central intensities that are not constant along the propagation distance. We present a technique for converting a Gaussian beam to a J_1 -like hollow beam, efficiently with a constant central intensity, using an amplified holographic reconstruction technique. The hollow beam, which is obtained by modification of a J_0 beam, is not identical to a J_1 beam but is very similar to it. Durnin's original configuration [1,2] for generating J_0 beams has serious energy loss associated it. More efficient conversions were demonstrated using computer-generated holograms, which enable one to produce Bessel beams of a order higher than the J_0 beam [7,8]. The drawback of the holographic technique is the relative nonuniformity of the central intensity along the propagation distance as compared with Durnin's configuration. An axicon [9] provides an alternate technique for producing these beams (see Herman and Wiggins [10]). With an axicon alone one can produce a J_0 beam with an efficiency close to 1. However, as is the case with the computer-generated hologram, the axicon method has a nonuniform central intensity along the propagation distance. This problem can be removed by proper apodization [10]. Uniformity along the propagation distances, with high efficiency, can be achieved by a simple amplification techniques of Durnin's J_0 beam, using either two-wave mixing [11] or amplified holographic reconstruction [12,13]. We will use the latter technique to show that a nondiffracting hollow (J_1 -like) beam can be generated efficiently by the modification of a J_0 beam.

DISCUSSION

Durnin [1] showed that the J_0 beam has the form of $J_0(\alpha\rho)$, where ρ is a radial distance. $J_0(x)$ can be expressed as

$$J_0(x) = \frac{1}{2\pi} \int_0^{2\pi} e^{ix\sin\theta} d\theta, \tag{1}$$

which comes from the more general form [14],

$$J_n(x) = \frac{1}{2\pi} \int_0^{2\pi} e^{i(x\sin\theta - n\theta)} d\theta, \tag{2}$$

or, alternatively, from

$$J_n(x) = \frac{i^{-n}}{2\pi} \int_0^{2\pi} e^{i(x\cos\theta + n\theta)} d\theta. \tag{3}$$

Comparing Eq. (1) to Eq. (2) or Eq. (3) we see that higher-order Bessel beam can be achieved with an additional phase factor $e^{-in\theta}$ or $e^{in\theta}$. Therefore, the J_1 beam can be written as

$$\begin{aligned} J_1(x) &= \frac{1}{2\pi} \int_0^{2\pi} e^{i(x\sin\theta - \theta)} d\theta \\ &= \frac{1}{2\pi} \int_0^{2\pi} e^{-i\theta} e^{ix\sin\theta} d\theta. \end{aligned} \tag{4}$$

Or, if we use Eq. (3) as a starting point,

$$\begin{aligned} J_1(x) &= \frac{1}{2\pi i} \int_0^{2\pi} e^{i(x\cos\theta + \theta)} d\theta \\ &= \frac{1}{2\pi i} \int_0^{2\pi} e^{+i\theta} e^{ix\cos\theta} d\theta. \end{aligned} \tag{5}$$

Experimentally, the addition of the $e^{\pm i\theta}$ phase factor inside the integrals [Eqs. (4) and (5)] can be achieved by adding a circular wedged phase plate to Durnin's configuration [Fig. 2(a)]. This phase plate could consist

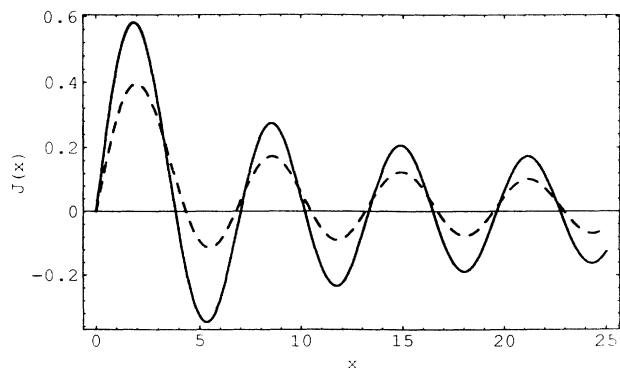


FIG. 1. Comparison of the $J_1(x)$ (solid curve) and $J_{11}(x)$ (dashed curve).

of a disk whose optical thickness increases linearly with angle. Alternatively, Durnin's annular slit can be replaced with a wedged annular slit. Such circular phase plates are not commercially available. Hence, it is difficult in practice to produce the J_1 beam. We devised a technique for obtaining a J_1 -like hollow beam, which we shall denote as $J_{1'}$.

An annular slit can be considered as a limiting case of an n polygon as n becomes infinite. Thus, the diffraction pattern of an angular slit is a diffraction pattern of the n polygon in the limit of $n \rightarrow \infty$. Each polygon consists of two opposite sides. The two sides form a double-slit diffraction pattern whose intensity distribution is

$$I(\theta) = (\sin\beta/\beta)^2 \cos^2\gamma, \quad (6)$$

where $I(\theta)$ is the intensity at an angle of θ from the line of incidence, $\beta = \frac{1}{2}kb \sin\theta$ (b is the slit width), $\gamma = \frac{1}{2}kh \sin\theta$ (h is the slit separation), k is the wave number. For $b < h$ the first factor $(\sin\beta/\beta)^2$ is an envelope function. For this distribution, b is very narrow and the slit length should be very large as a condition of the double-slit pattern. In an n -polygon slit, the slit length is finite, hence the diffraction pattern will show azimuthal angle dependence. But in an annular slit, which is a limit of an n polygon, there is no azimuthal dependence (circularly uniform), hence we need not consider this effect.

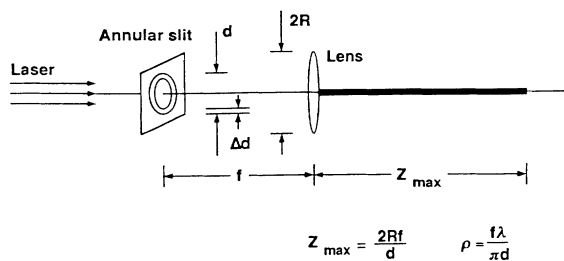
In a double-slit experiment when one side is half-wavelength retarded, the intensity distribution changes as

$$I(\theta) = (\sin\beta/\beta)^2 \sin^2\gamma. \quad (7)$$

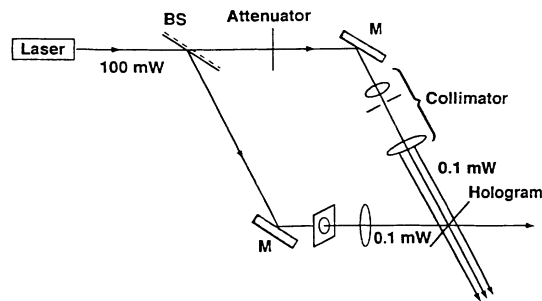
That is, the dark fringes are changed to bright and vice versa. Equation (6) exhibits a bright central position, while Eq. (7) shows central darkness. Both these beams spread, fanning out due to the sine factor. The dark and bright fringe lines corresponding to $\cos\gamma$ or $\sin\gamma$ follow asymptotic lines originating at the center of the two slits. Placing a lens at a distance of one focal length, f , beyond the slits, has the consequence that all the asymptotic lines associated with $\cos\gamma$ or $\sin\gamma$ will emerge parallel along the axis after the lens, since all the lines originated at the same point. The envelope function which arises from the slit width, b , will now spread along the direction connecting a slit point and the center of lens. This occurs because the lens acts as a Fourier-transform lens, and every point in the object is converted to a directional beam. The envelope will cross the lens axis, thus affecting the intensity along the lens axis. The lens diameter will restrict the intensity along the lens axis if its diameter does not cover the entire envelope. These considerations indicate that the intensity along the axis is dependent on the slit distance, slit width, focal length, diameter of the lens, and the wavelength. The n -polygon slits, with a lens, will show a cylindrical fringe pattern along the lens axis. The central axis will be very bright, the sum of the contributions of each double slit of the polygon. If half of the n -polygon sides are half-wavelength retarded, then the central position will be dark, and the intensity distribution will be reversed. The same principle applies for an annular slit, except for the addition of circular symmetry. If half of the annular slit is phase retarded by half wavelength it will generate a hollow beam similar to the J_1 beam near the lens axis. However, it will not be identical to J_1 because J_1 is produced by the phase factor $e^{i\theta}$. The difference between J_1 and $J_{1'}$ can be demonstrated by considering the factor $e^{ix\sin\theta}$ as follows [14]:

$$\begin{aligned} e^{ix\sin\theta} = & J_0(x) + 2[J_2(x)\cos 2\theta \\ & + J_4(x)\cos 4\theta + J_6(x)\cos 6\theta + \dots] \\ & + 2i[J_1(x)\sin 1\theta + J_3(x)\sin 3\theta \\ & + J_5(x)\sin 5\theta \dots]. \end{aligned} \quad (8)$$

(a) Generation of J_0



(b) Holographic Amplification



(c) Holographic Addition

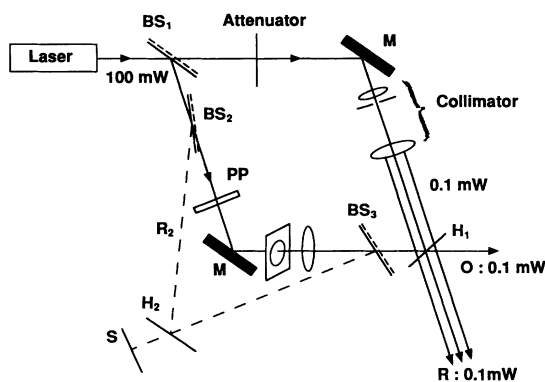


FIG. 2. Generation and amplification of $J_{1'}$. (a) Production of J_0 , (b) Holographic amplification, and (c) the combination of the two processes to form holographic addition. M , BS , PP , and H are mirror, beam splitter, phase plate, and hologram, respectively. $2R$ is the lens diameter, f the focal length, d the annular slit diameter, and Δ the annular slit width.

An annular slit with a phase plate in front of it will generate a beam pattern $J_{1'}$ that can be represented by Eq. (1) plus the additional phase factor $e^{i\phi(\theta)}$ (due to the phase plate) in the integrand, i.e.,

$$J_{1'}(x) = \frac{1}{2\pi} \int_0^{2\pi} e^{i\phi(\theta)} e^{ix\sin\theta} d\theta. \quad (9)$$

The phase function $\phi(\theta)$, giving half-wavelength retardation, is

$$\phi(\theta) = \begin{cases} 0 & \text{for } 0 < \theta < \pi \\ \pi \pm 2n\pi & \text{for } \pi < \theta < 2\pi, \end{cases}$$

n is an integer. The corresponding phase factor, $e^{i\phi(\theta)}$, becomes,

$$e^{i\phi(\theta)} = \begin{cases} e^{i0} = +1 & \text{for } 0 < \theta < \pi \\ e^{i(\pi \pm 2n\pi)} = -1 & \text{for } \pi < \theta < 2\pi. \end{cases}$$

Integrating Eq. (9) by parts,

$$J_{1'}(x) = \frac{1}{2\pi} \int_0^\pi e^{ix\sin\theta} d\theta - \frac{1}{2\pi} \int_\pi^{2\pi} e^{ix\sin\theta} d\theta, \quad (10)$$

and recalling the basic formulas for even n ,

$$\int_0^\pi \cos(n\theta) d\theta = \int_\pi^{2\pi} \cos(n\theta) d\theta = 0, \quad (11)$$

and for odd n ,

$$\int_0^\pi \sin(n\theta) d\theta = +\frac{2}{n} \quad (12)$$

and

$$\int_\pi^{2\pi} \sin(n\theta) d\theta = -\frac{2}{n}. \quad (13)$$

We have, upon combining Eqs. (10) and (8),

$$J_{1'}(x) = \frac{2}{\pi} [J_1(x) + \frac{1}{3}J_3(x) + \frac{1}{5}J_5(x) + \dots]. \quad (14)$$

We see that $J_{1'}(x)$ is proportional to $J_1(x)$ plus all higher orders of odd $J_n(x)$ weighted by the order number n . In many experiments, such as light-particle interaction, one may be interested mainly in the region within the first maximum ($x = 1.8412$) of J_1 beam. Within this range, $J_1(x) > J_n(x)$ and $J_n(x) > J_{n+2}$. All higher orders are similarly weighted, thus $J_{1'}$ is close to J_1 .

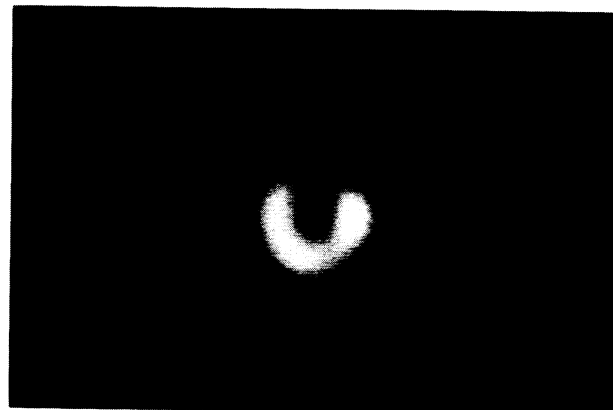
Figure 1 compares the $J_1(x)$ and $J_{1'(x)}$ values for small x up to $n = 17$. The first maximum position of $J_{1'}$ is at a slightly larger value of x than that of J_1 . Because all $J_n(n > 1)$ are monotonic and have positive values in the range ($x < 1.8412$), the slope of $J_{1'}$ is slightly larger than the factor $2/\pi$.

In light interaction with particles, the usual beam pattern is a plane wave of a Gaussian TEM₀₀ mode beam. This beam is given by [15]

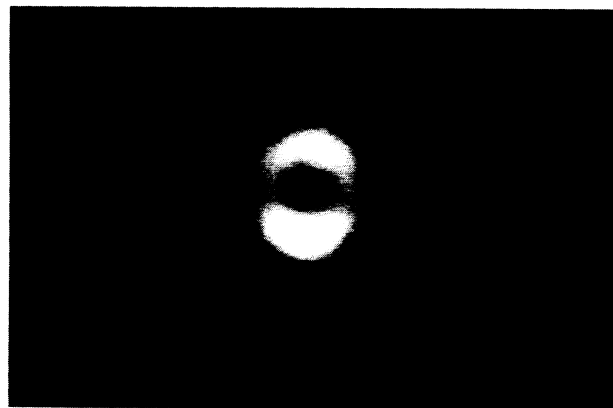
$$I_G(r, z) = I_{0,G} e^{-2r^2/w^2(z)} = \frac{2P_t}{\pi w^2(z)} e^{-2r^2/w^2(z)}, \quad (15)$$

where P_t is total power, and $w(z)$ is the spot size parameter of the Gaussian beam which increases with z . Unlike a plane wave, this Gaussian beam spreads as it propa-

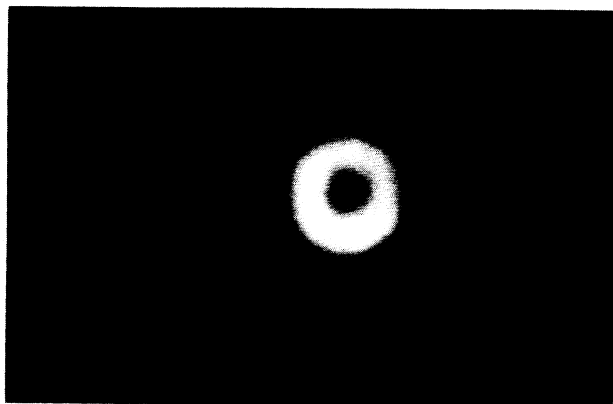
gates, and it has a negative gradient force along the radial distance near the axis. In this case the particles are concentrated at the highest light intensity, resulting in diffusion. The TEM₀₁* mode (doughnut mode), which is the first excited circular mode, has a positive gradient along the radial distance near the center and may be used with opposite detuning compared to the TEM₀₀ [16,17],



(a)



(b)



(c)

FIG. 3. The central intensity of the J_0 beam. Holographic addition of (a) and (b) results in (c). Higher-order rings are too weak to be seen.

for tight focusing of the particle. However, this beam also has the same spreading factor [15]:

$$I_{\text{TEM}_{01}^*}(r, z) \propto r e^{-2r^2/w^2(z)}. \quad (16)$$

Bessel beams, on the other hand, do not have spreading factors. Hence, they propagate without energy loss, although they usually have long tails along the radial distance. They may, however, have gradients of higher slopes, as will be shown below.

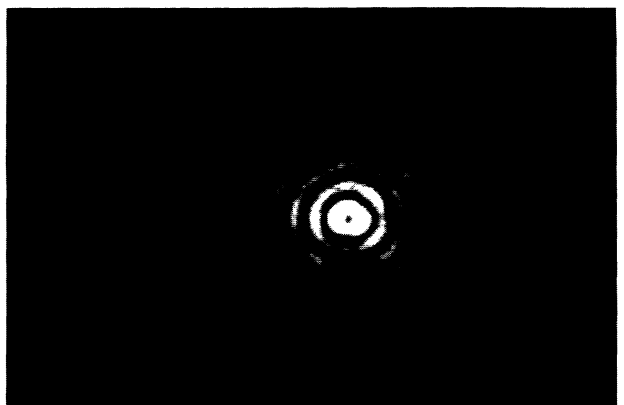
EXPERIMENT

Figure 2 shows the production and amplification of $J_{1'}$. The amplification of the beam is based on holographic amplification-reconstruction technique [6] of low static optical fields. The phase plate (PP) [in Fig. 2(c)] has a uniform thickness. A half-wavelength phase difference is achieved by adjusting the effective thickness with slight tilting of the plate. In our experiment we used a glass microscope slide of 0.25-mm thickness. This is not an ideal substitute for a parallel plate, but it gave acceptable results. The nonuniformity of the slide, as well as edge effects of the phase plate resulted in the $J_{1'}$ beam pattern not being circularly symmetric. These circular fluctuations can be averaged by the addition of another rotated image. Figure 2(b) is a 90° rotated beam with respect to

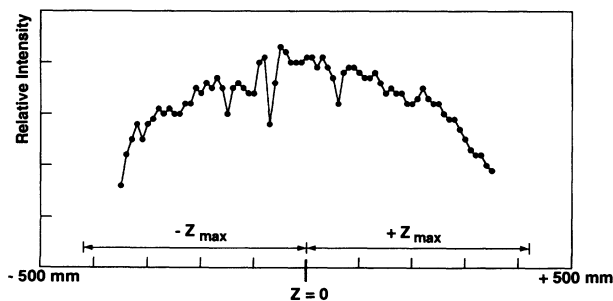
Fig. 2(a), while Fig. 2(c) combines the features of Figs. 2(a) and 2(b). In order to accomplish the holographic addition, auxiliary beam splitters BS_2 , BS_3 , and holographic plate, H_2 , were used. Holograms H_1 and H_2 were initially exposed at the same time. First H_2 was developed and repositioned, while H_1 was kept shielded from light. The two beams are projected and superimposed on screen S . One beam is the original signal beam and the other is an image beam generated by reference beam R_2 , of hologram H_2 . Rotating phase plate, PP, will rotate the signal beam pattern alone, leaving the image beam unchanged. The rotated signal beam, reexposed on H_1 , averages out the circular fluctuations.

We used an Ar^+ laser of wavelength 514.5 nm and spot size (e^{-2} point) of 1.1 mm. Figure 3 shows the central intensity of the J_0 beam which serves as the source of the $J_{1'}$ beam in the range $-Z_{\text{max}} - +Z_{\text{max}}$ obtained for the optical setup of Fig. 2(c). The dimensions of our setup are as follows: annular slit diameter $d = 2.5$ mm, annular slit width $\Delta d = 10 \mu\text{m}$, lens focal length $f = 140$ mm, lens diameter $2R = 7.5$ mm. These parameter gave a first zero ring diameter of $2r = 44.1 \mu\text{m}$. The measured value is closed to this value and uniform along the propagation distance.

The calculated first zero ring diameter, for the $J_{1'}$ beam, is $75.6 \mu\text{m}$ while the measured values were in the



(a)

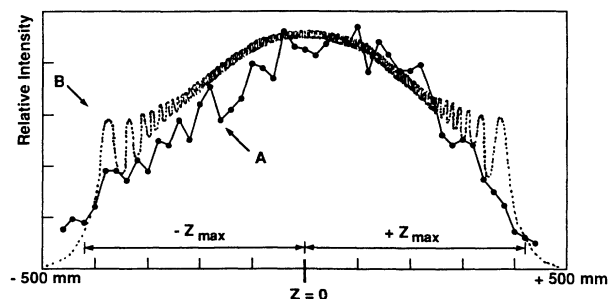


(b)

FIG. 4. (a) A photograph of the $J_{1'}$ beam (note that the central portion is over saturated). (b) Relative intensities of the central peak along the z axis. Measured values are connected with solid lines. (Note the flattening compared to J_0 in Fig. 5.)



(a)



(b)

FIG. 5. (a) A photograph of J_0 beam (note that the central portion is over saturated). (b) Relative intensities of the central peak along the z axis. The dashed curve is a computer simulation of estimated values. The solid curve connects points of measured values.

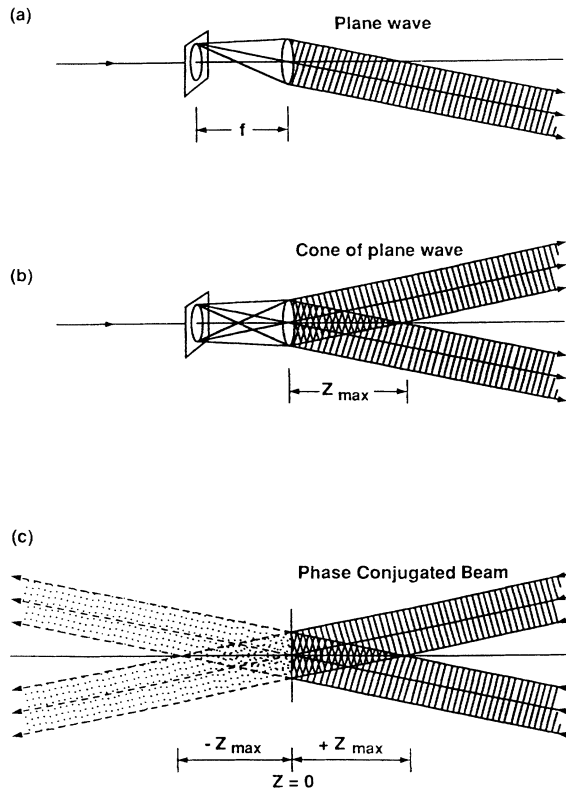


FIG. 6. Geometrical construction of the Bessel beam. (a) A point in the annular slit becomes a parallel plane wave. (b) An annular slit and a lens generate a cone of plane waves. (c) The phase conjugated cone of the cone of plane waves is a symmetric extended beam, when one removes the lens and the slit.

range 70.3–78.0 μm . The total power within this first ring is shown in Fig. 4. We assume that this power is proportional to the maximum intensity of the first bright ring. Note the relatively constant value of this intensity compared to the value of J_0 in Fig. 5. This uniformity is easily achieved with ordinary holography. The intensity near Z_{\max} is determined by rays coming from marginal part of the lens where the intensity is lower because of either finite Δd , or short focal length f (see Fig. 6). The reconstructed holographic efficiency is dependent on fringe contrast of the hologram. One may adjust the reference beam level such that the hologram produces higher diffraction efficiency near Z_{\max} , thus producing a relatively uniform central intensity along the propagation distance. The reference beam level, in taking the hologram for J_0 , was higher than any part of the signal beam, so the reconstructed beam is proportional to original (object) signal beam. On the other hand, for the hologram of the $J_{1'}$ beam, the reference beam level was close to the weakest part of the signal beam. Because of the lower contrast, the brightest part of the original signal beam, upon reconstruction, had low efficiency. This gives rise to the uniform intensity along the propagation distance.

The overall conversion efficiency of the Gaussian beam to the Bessel beam was about 50% [13]. In our setup the Bessel beams contained about 130 zero rings. Since each zone of rings has approximately the same energy, we may calculate the peak intensity for J_0 as

$$I_{0,J} = 0.5 \frac{P_t}{130} \frac{1}{\pi \rho_0^2} = 0.5 \frac{I_{0,G}}{2} \frac{1}{130} \frac{w^2}{\rho_0^2} = I_{0,G} \frac{1}{520} \frac{w^2}{\rho_0^2}, \quad (17)$$

where ρ_0 is a spot parameter of the central ring of $J_0(ar)$ and is approximately $1/\alpha$ [1]. If we compare the half energy spot size, w , of the Gaussian to that of J_0 , we find $w/\rho_0 \approx 65$, so $I_{0,J} > I_0$, and for the $J_{1'}$ beam, $I_{0,J_{1'}} \approx 0.4 I_{0,J_0}$.

CONCLUSION

We believe that these beams may be useful for particle beam interaction as well as isotope separation. The size of the first ring diameter is easily controlled by projection through a combination of negative and positive lenses [10]. Sharp focusing of central spot is also possible [18]. Thus, very narrow particle beams, collimated by the gradient force of either J_0 (positive detuning) or $J_{1'}$ (negative detuning) is possible. The gradient of the intensity of the Gaussian beam of Eq. (15) is

$$\begin{aligned} \frac{d}{dr} I_G(r, z) &= I_{0,G} \frac{-2r}{w^2(z)} e^{-2(r^2)/w^2(z)} \\ &= -I_{0,G} (2r) w^{-2} \quad r \ll 1. \end{aligned} \quad (18)$$

If we take the same peak intensity for the J_0 , or the $J_{1'}$ beam as that of the Gaussian beam (and assuming that the intensity of $J_{1'} \approx J_1$), then

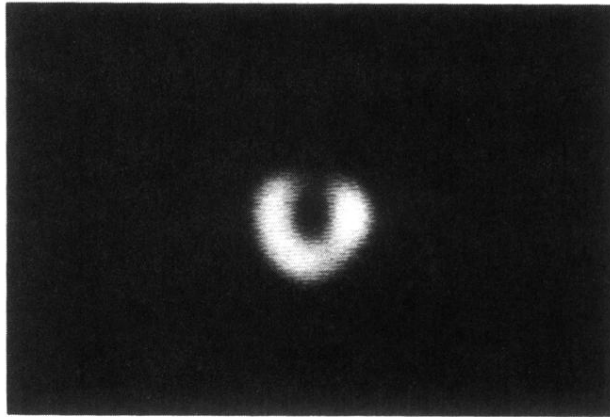
$$\begin{aligned} \frac{d}{dr} I_{J_0} J_0^2(ar) &= \frac{d}{dr} I_{0,G} J_0^2(ar) \\ &= I_{0,G} (-2\alpha) J_0(ar) J_1(ar) \\ &= -I_{0,G} r \rho^{-2} \quad r \ll 1, \end{aligned} \quad (19)$$

while for $J_{1'}$,

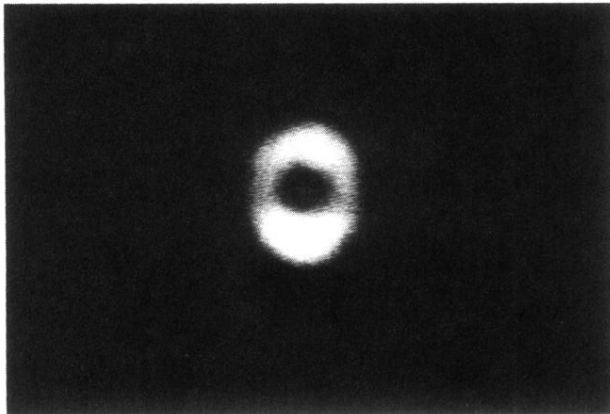
$$\begin{aligned} \frac{d}{dr} I_{J_{1'}} J_{1'}^2(ar) &= \frac{d}{dr} I_{0,G} J_{1'}^2(ar) \\ &= I_{0,G} 2\alpha J_1(ar) \frac{1}{2} [J_0(ar) - J_2(ar)] \\ &= I_{0,G} (0.5r) \rho^{-2} \quad r \ll 1. \end{aligned} \quad (20)$$

Note that ρ in Eq. (20) is same as that in Eq. (19). We see that the gradient force, which is inversely proportional to the central spot size, is much larger for the Bessel beams than Gaussian. In conclusion, we have demonstrated that the hollow beam $J_{1'}$ is close to the Bessel beam $J_{1'}$. Such beams are not difficult to obtain experimentally and, thus, may be useful in such areas as particle collimation.

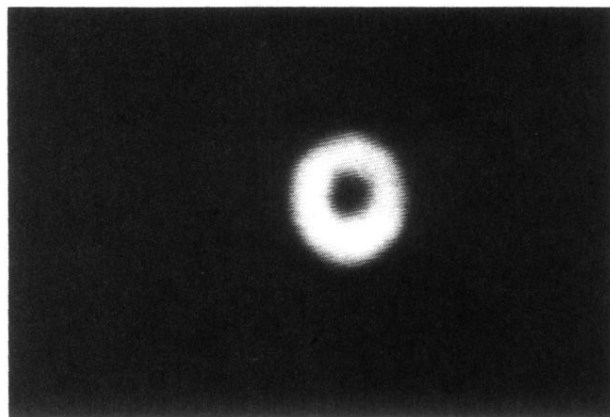
- [1] J. Durnin, *J. Opt. Soc. Am. A* **4**, 651 (1987).
- [2] J. Durnin, J. J. Miceli, and J. H. Eberly, *Phys. Rev. Lett.* **58**, 1499 (1987).
- [3] F. Bloisi and L. Vicari, *Opt. Commun.* **75**, 353 (1990).
- [4] S. De Nicola, *Opt. Commun.* **80**, 299 (1991).
- [5] A. J. Cox and Dean C. Dibble, *Appl. Opt.* **30**, 1330 (1991).
- [6] Hee S. Lee, B. W. Stewart, D. Will, and Henry Fenichel, *Appl. Phys. Lett.* **59**, 1 (1991).
- [7] J. Turunen, A. Vasara, and T. Friberg, *Appl. Opt.* **27**, 3959 (1988).
- [8] Antti Vasara, Jari Turunen, and Ari T. Friberg, *J. Opt. Soc. Am. A* **6**, 1748 (1989).
- [9] J. H. McLeod, *J. Opt. Soc. Am.* **44**, 592 (1954).
- [10] R. M. Herman and T. A. Wiggins, *J. Opt. Soc. Am. A* **8**, 932 (1991).
- [11] B. W. Stewart, US Patent No. 4,992,750 (18 July 1989).
- [12] Hee S. Lee, David Will, and Henry Fenichel, *Appl. Opt.* **30**, 5147 (1991).
- [13] Integraf, P. O. Box 586, Lake Forest, IL 60045.
- [14] G. Arfken, *Mathematical Methods for Physicists* 2nd ed. (Academic, New York, 1970), pp. 478–492.
- [15] H. Kogelnik and T. Li, in *Laser Theory*, edited by Frank S. Barnes (IEEE, New York, 1972), pp. 97–114.
- [16] G. M. Gallatin and P. L. Gould, *J. Opt. Soc. Am. B* **8**, 502 (1991).
- [17] Hee S. Lee, B. W. Stewart, K. Choi, and H. Fenichel, in *Proceedings of the International Conference on Lasers '91, San Diego, California, 1991*, edited by F. J. Duarte and D. G. Harris (STS, McLean, 1992), pp. 588–594.
- [18] Hee S. Lee, B. W. Stewart, and Henry Fenichel (unpublished).



(a)

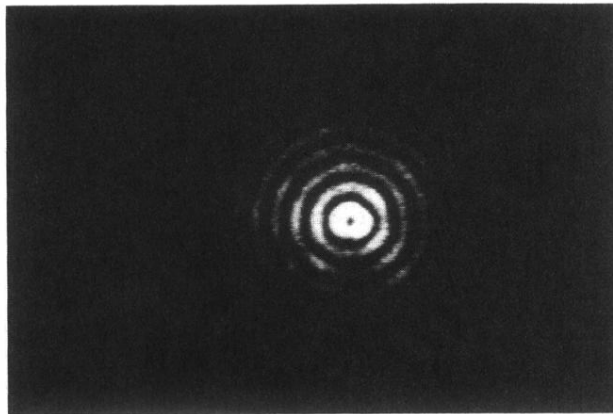


(b)

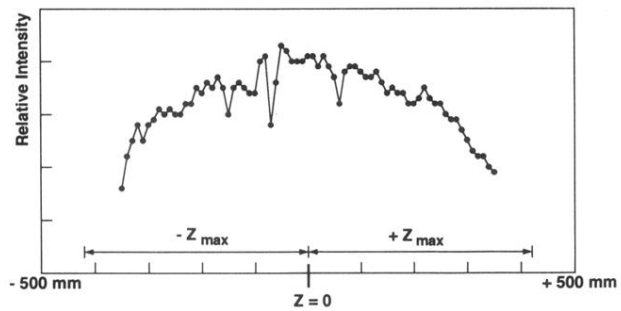


(c)

FIG. 3. The central intensity of the J_0 beam. Holographic addition of (a) and (b) results in (c). Higher-order rings are too weak to be seen.

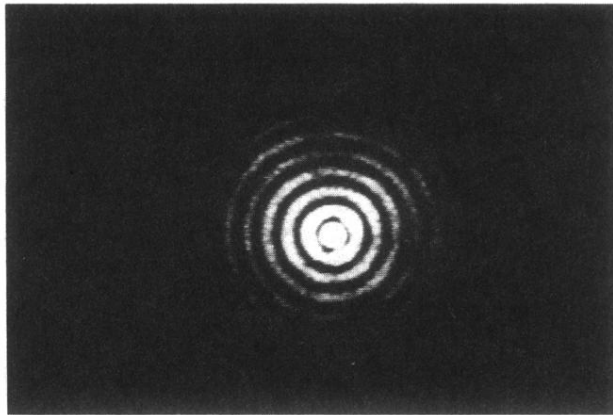


(a)

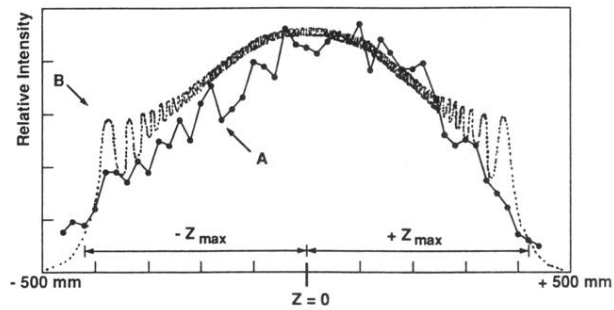


(b)

FIG. 4. (a) A photograph of the $J_{1'}$ beam (note that the central portion is over saturated). (b) Relative intensities of the central peak along the z axis. Measured values are connected with solid lines. (Note the flattening compared to J_0 in Fig. 5.)



(a)



(b)

FIG. 5. (a) A photograph of J_0 beam (note that the central portion is over saturated). (b) Relative intensities of the central peak along the z axis. The dashed curve is a computer simulation of estimated values. The solid curve connects points of measured values.